A Numerical Method for the Viscoelastic Melt-Spinning Model with Radial Resolutions of Temperature and Stress Fields

Mariel L. Ottone and Julio A. Deiber*

Instituto de Desarrollo Tecnológico para la Industria Química, INTEC (UNL-CONICET), Güemes 3450, 3000 Santa Fe, Argentina

A numerical method to compute the viscoelastic melt-spinning model with radial resolutions of temperature and stress fields is formulated and applied to the low speed range. The starting framework is the reduction of the complete continuous model into both the perturbed two-dimensional model and the perturbed average model obtained from a first-order regular perturbation analysis available in the literature. The polymer rheology is described with the nonisothermal Phan-Thien and Tanner and Giesekus constitutive equations. By using the implicit tridiagonal scheme of finite differences coupled to the fourth-order Runge−Kutta method, an iterative numerical algorithm is proposed for the computation of the coupled balance equations. The temperature and stress fields in the filament as functions of axial and radial positions are obtained for a well-refined mesh and with high numerical precision. The numerical algorithm considers the appropriate interplay between axial and radial varying temperature and stress fields and the rigorous averaged balances of momentum and energy and averaged constitutive equation. The development of a skin-core structure is predicted with the two rheological models.

Introduction

In fiber melt spinning, a bunch of polymer melt filaments are continuously drawn and simultaneously cooled with air in order to obtain solidified yarns, which later compose the synthetic fiber in the bobbin (Figure 1 shows a scheme for this operation involving one filament only). Melt spinning is a basic nonisothermal operation in the production of synthetic fibers (see, for example, Denn[1,2] and Schowalter[3]), and hence a model describing the velocity, stress and temperature fields in the filaments can be useful to control the quality of the final product. Nevertheless, this model is rather complex because it shall involve basically the balance equations of momentum and energy coupled to appropriate nonisothermal constitutive equations of the polymeric material. The filament also presents a free surface that must be determined together with the field solutions, introducing thus an additional complexity into the model.

In fiber melt spinning, the radial and axial variations of stresses and temperature are believed to control strongly the mechanical and physical properties of fibers obtained under specific thermal operating conditions. In the last years, researches were placing emphasis on the quantification of this particular aspect when a model for the fiber spinning process was proposed. In this sense, Henson et al.[4] have studied a model for the fiber spinning operation to account for the most relevant phenomena associated with a two-dimensional (2D) description of temperature and stress fields. This model was formulated for the low speed range (flow-induced crystallization was not considered) through a regular perturbation analysis that included the slenderness approximation associated with long fibers of very small diameters. These authors analyzed deeply the mathematical structure of the perturbed 2D model including its relation with the classical one-dimensional (1D) model that resulted from the radial average of momentum and energy balances and constitutive equation. It was found analytically that a first-order axial velocity radially uniform could be computed within the same order of magnitude with a radially varying temperature, which was responsible for the radial variations of stresses in the fiber. These authors illustrated the 2D model by assuming, as a first approximation, that the melt was a Newtonian fluid. Their results were important to yield a robust model structure, allowing one to quantify the interplay between the operational variables in fiber melt spinning and the axial and radial temperature and stress fields. Therefore, one can use a simpler version of the complete 2D model that may be rather complex to solve at the present time.

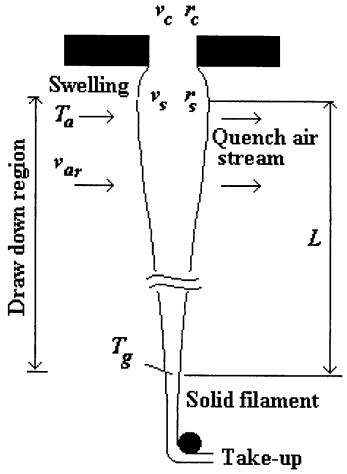

Figure 1. Scheme of the spinning operation for one filament.

More recently, Doufas and McHugh[5] studied the fiber melt-spinning operation under the same mathematical structure of the 2D model proposed by Henson et al.[4] with the inclusion of the flow-induced crystallization (FIC) phenomenon that is important mainly for the high speed range of take-up velocities (velocities greater than

* To whom correspondence should be addressed. Tel: 54 342 4559174/77. Fax: 54 342 4550944. E-mail: treoflu@ceride.gov.ar.

10.1021/ie011001i CCC: $22.00
Published on Web 06/07/2002

3000 m/min). For this case, two coupled constitutive equations were necessary:[6] one for the flow-induced crystallized phase and the other for the ordering amorphous phase in the elongational flow field. The relevant parameter for the coupling mechanism, apart from the temperature field, was the degree of crystallization evaluated through a modified Avrami equation. Apart from describing the relevant fields in the filament, these authors also predicted phenomena present in fiber melt-spinning operations such as the skin-core structure.

From the above analysis, it is clear that the radial and axial stress and temperature fields in fiber melt spinning may be estimated within a consistent theoretical framework of a perturbed 2D model that uses the slenderness approximation for both low and high speed ranges. For this purpose, robust numerical algorithms computing the resulting momentum and energy balances coupled to constitutive equations are also useful. Otherwise, one exploits partially the potentiality of the perturbed 2D model. Several works have used additional hypotheses by considering the average mass and momentum balances and average constitutive equation in order to be able to compute a 2D temperature field within the consistent mathematical structure described above (hybrid 1D fluid mechanics/2D thermal models, as designated by Doufas and McHugh[5]). For these calculations, approximations associated with the average of terms involving temperature and stresses are required. Without these hypotheses, the method of lines, which uses a polynomial approximation for the radial and axial variations of the temperature and stress fields, was used more recently to evaluate the perturbed 2D model with both viscoelastic melt and flow-induced crystallization (two-fields model).[5] Polynomials of fourth order were used to reach the desired precision.

One of the purposes of our work is to show here that, within the structure of the perturbed 2D model discussed above, an iterative numerical algorithm can be generated to compute the axial varying velocity coupled to the axial and radial temperature and stress fields in the filament by using finite differences. With this specific target, we use the analytical coupling between the perturbed average model resulting from the rigorous radial average of the perturbed 2D model and the associated pointwise energy balance and constitutive equations for stresses. The perturbed average model is solved with the Runge−Kutta method, and the 2D balances are solved through finite differences, both coupled iteratively at each axial step and fulfilling convergence criteria. The finite difference equations involve the implicit tridiagonal algorithm for the temperature field and the explicit−implicit backward differences for the stresses. Fine meshes can be generated to the desired precision (for instance, 100 radial nodes and axial step sizes of 10^{-5}, with these aspects depending on the precision and details required). In this work, we consider the low speed range of fiber spinning by following strictly the 2D model proposed by Henson et al.[4] and FIC is not accounted for. In this sense, it is clear that, for the case considering FIC, the model must include an additional constitutive equation and the rate of crystallization presented already by Doufas and McHugh.[6]

In addition, the numerical method is illustrated with two different viscoelastic constitutive equations: Phan-Thien and Tanner and Giesekus models. The viscoelastic polymer is described through two mechanical contributions to the extra stress tensor $\boldsymbol{\tau} = \boldsymbol{\tau}_s + \boldsymbol{\tau}_p$. One of them considers a Newtonian response, $\boldsymbol{\tau}_s$, in general attributable to the retardation effects of the macromolecular structure in the viscoelastic relaxation phenomena. The other contribution, $\boldsymbol{\tau}_p$, describes the instantaneous elastic response of the polymer in the sense discussed by Denn.[7] The retardation effects included in these rheological models allowed us to introduce the initial conditions of the spinning model at a well-specified position in the fiber, as is described below (see also Ottone and Deiber[8]). In these models the thermal history is considered through the term $D \ln T/Dt$, which involves the rate of change of temperature.[9,10] In addition, the polymer heat capacity c_v, the relaxation time λ, and the relaxation modulus G are considered functions of temperature. Numerical results are validated with experimental data of the spinning process reported for a poly(ethylene terephthalate) (PET).

Basic Equations

In this section we present the so-called complete model, which is formulated for the steady-state regime. Because the polymer is considered incompressible, the mass balance implies

$$(\nabla \cdot \mathbf{v}) = 0 \tag{1}$$

where $\mathbf{v}$ is the velocity vector. The balance of momentum in the filament is expressed as

$$\rho \mathbf{v} \cdot \nabla \mathbf{v} = -\nabla p + \nabla \cdot \boldsymbol{\tau} + \rho \mathbf{g} \tag{2}$$

where ρ is the polymer density, p is the pressure field, $\mathbf{g}$ is the gravity vector, and $\dot{t}$ is the extra stress tensor considered symmetric throughout this work. The energy balance in the filament is

$$\rho c_v \mathbf{v} \cdot \nabla T = -\nabla \cdot \mathbf{q} + \mathbf{D}:\dot{\boldsymbol{t}} \tag{3}$$

where $c_v = a + bT$ is the polymer thermal capacity and T is the temperature field (temperature T is expressed in degrees Celsius throughout this work). In eq 3, $\mathbf{q} = -k_s \cdot \nabla T$ is the heat flux vector, k_s is the thermal conductivity, and $\mathbf{D}:\boldsymbol{\tau}$ is the mechanical power. This term involves the rate of deformation tensor $\mathbf{D} = (\nabla \mathbf{v} + \nabla \mathbf{v}^T)/2$, which is a function of the fluid kinematics $\mathbf{v}(r,z) = v_z \mathbf{e}_z + v_r \mathbf{e}_r$, where v_z and v_r are the axial and radial components of the velocity vector, respectively, in the cylindrical coordinate system. Here the angular component of the velocity vector is null because no perturbation in the flow field is considered.

The appropriate set of boundary conditions to solve eqs 1−3 is taken directly from Denn.[2] In addition, because in our model the PTTM and GM are considered with the retarded elastic response (the term $\boldsymbol{\tau}_s = 2\eta_s \mathbf{D}$ is included), initial values for τ_s^{zz} and τ_s^{rr} are needed at $z = 0$, apart from the stress τ_p^{zz} and the relation $\mathrm{Rel} = \tau_p^{rr}/\tau_p^{zz}$ already discussed in the literature.[2] This requirement is equivalent to the assignment of a value to the velocity derivative at $z = 0$. This additional initial condition was expressed as $\partial v_z/\partial z \approx 0$, which is an estimate for the velocity derivative at the maximum filament swelling.[8] In fact, it was found with the PTTM that, for $\partial v_z/\partial z \rightarrow 0$, the numerical solutions obtained for the average temperature and velocity of the filament were not dependent on the small values assigned to this derivative. On the other hand, when this rheological

model with instantaneous elastic response was used (the term $2\eta_s\mathbf{D}$ was not included), the condition $\partial v_z/\partial z \approx 0$ is not satisfied for any assumed initial filament radius, and hence, the position $z = 0$ is not well determined in relation to the capillary exit. Usually, authors suggest in this case to put it around 2−4 capillary diameters below the capillary exit.[11]

In the sense discussed above, we fix the origin of the coordinate system at the maximum swelling of the polymer melt, where the jet forms at the exit of the extrusion capillary. At this place the properties are assumed to be uniform in the radial direction.[2] Therefore, throughout this work we designate initial conditions to the boundary conditions at $z = 0$, which for any value of r are

$$v_z = v_s, \quad T = T_0, \quad \tau_s^{zz} = \tau_s^{rr} = 0$$

$$r_0(0) = r_s, \quad \tau^{zz} = \tau_0^{zz}, \quad \mathrm{Rel} = \frac{\tau^{rr}}{\tau^{zz}} \tag{4}$$

where $r_0(z)$ is the fiber radius as a function of the axial direction z, v_s is the melt velocity at the maximun swelling with radius r_s, and T_0 is the extrusion melt temperature. Thus, $v_s = v_c r_c^2/r_s^2$ where v_c is the melt-averaged velocity in the extrusion capillary of radius r_c. Also the stress ratio Rel can be varied in the range $-1/2 < \mathrm{Rel} < 0$ for viscoelastic fluids. This result has been fully discussed in the literature,[2] where it was reported that numerical solutions were not sensitive for values of Rel within this specific range and that the condition Rel ≈ 0 is a good approximation.[12,13] Nevertheless, one should also consider that the initial stress required for a viscoelastic model must be determined more rigorously by the flow history of the material prior to spinning. In this sense, the kinematics assumptions leading to the thin filament equations are not valid for the portion of the history prior to the spinneret, as was clearly stated in the revision work by Denn.[2] Therefore, this mechanical aspect is, in some degree, captured with the imposition of the initial filament radius, which, in principle, can be correlated with the first normal stress difference and the shear stress associated with the material flowing through the extrusion capillary (in this work it is the maximum swelling).

Boundary conditions involving the symmetry of fields are imposed at the center line $r = 0$ for any position z. Thus,

$$\frac{\partial v_z}{\partial r} = 0, \quad \frac{\partial T}{\partial r} = 0, \quad \frac{\partial \tau^{zz}}{\partial r} = 0, \quad \frac{\partial \tau^{rr}}{\partial r} = 0 \tag{5}$$

while at the filament free surface for $r = r_0(z)$ and any position z, dynamics and kinematics constraints are

$$(\mathbf{T}\cdot\mathbf{n})\cdot\mathbf{t} = (\mathbf{T}_a\cdot\mathbf{n})\cdot\mathbf{t} \tag{6}$$

$$(\mathbf{T}\cdot\mathbf{n})\cdot\mathbf{n} = -\sigma\aleph\mathbf{n}(\mathbf{T}_a\cdot\mathbf{n})\cdot\mathbf{n} \tag{7}$$

$$\mathbf{v}\cdot\mathbf{n} = 0 \tag{8}$$

$$\mathbf{v}\cdot\mathbf{t} = \mathbf{v}_a\cdot\mathbf{t} \tag{9}$$

for the mechanical variables and

$$\mathbf{q}\cdot\mathbf{n} = h_e\Delta T \tag{10}$$

for the temperature field. In these equations, $\mathbf{n}$ and $\mathbf{t}$ are the unit vectors normal and tangential to the free surface, respectively, $\aleph$ is the curvature of the free surface, and σ is the polymer−air surface tension. In addition, the stress tensor $\mathbf{T} = -p\boldsymbol{\delta} + \boldsymbol{\tau}$ involves the extra stress tensor and the pressure p, where $\boldsymbol{\delta}$ is the unit tensor. In eq 10, $\Delta T = T - T_a$ is the thermal jump between the average air temperature T_a used to cool the fiber (Figure 1) and the polymer temperature T evaluated at the free surface. h_e is the external coefficient of heat transfer to be analyzed below. We designate L as the length from the fiber maximum swelling to the position where the melt reaches the glassy temperature T_g, to become solidified. Also, τ_a^{nt} is the tangential extra stress at the fiber−air interface and $\mathbf{v}_a$ is the velocity vector, both of the cooling air.

In relation to eq 10, we are assuming that the model for the melt-spinning operation is uncoupled from the model of the quenching air, which may be an appropriate approximation when a monofilament spinning is considered, like in this work. This aspect has been analyzed and discussed thoroughly by Denn,[2] indicating that for the case of multifilament spinning additional considerations should be quantified. For instance, filament deflection is responsible for different air convections around the fiber. Also the cross-flow between air and filaments in the spinneret yields uneven cooling between different filament rows generating uneven lengths of filament solidification.

To complete the formulation of the spinning model, the viscoelastic stress $\boldsymbol{\tau}_p$ is required, which is a part of the total extra stress tensor $\boldsymbol{\tau} = \boldsymbol{\tau}_p + \boldsymbol{\tau}_s$, where $\boldsymbol{\tau}_s = 2\eta_s\mathbf{D}$ is associated with retardation effects. In this sense, one expresses

$$\boldsymbol{\tau}_p + \lambda_0\frac{\delta}{\delta t}\boldsymbol{\tau}_p + \frac{\alpha'}{G}(\boldsymbol{\tau}_p\cdot\boldsymbol{\tau}_p) = 2\lambda_0 G\mathbf{D} \tag{11}$$

for the Giesekus model (GM)[14] and

$$\boldsymbol{\tau}_p + \lambda\frac{\delta}{\delta t}\boldsymbol{\tau}_p = 2\lambda G\mathbf{D} \tag{12}$$

for the Phan-Thien and Tanner model (PTTM).[15] In eqs 11 and 12,

$$\frac{\delta}{\delta t}\boldsymbol{\tau}_p = \frac{D}{Dt}\boldsymbol{\tau}_p - \mathbf{L}\cdot\boldsymbol{\tau}_p - \boldsymbol{\tau}_p\cdot\mathbf{L}^T - \boldsymbol{\tau}_p\frac{D\ln T}{Dt} \tag{13}$$

is the Gordon−Schowalter[14,16] nonaffine time-convective derivative, where the effect of the thermal history is added through the term $D\ln T/Dt$. Also $\mathbf{L} = \nabla\cdot\mathbf{v} - \chi\mathbf{D}$ is the effective velocity gradient tensor ($\chi = 0$ for the GM). We define $\eta_s = \eta_p(1-\alpha)/\alpha$ and $\eta_p = \lambda G$; hence, the instantaneous elastic response of both models can be obtained for $\alpha = 1$.[7,17]

In relation to the last term of eq 13, one can find several works[18,19] indicating that the use of the time−temperature superposition principle alone is not enough to quantify the effect of a rapidly changing thermal history on the stress tensor. In this sense, one should not simply replace the relaxation time by a temperature-dependent function in the constitutive equations for the modeling of nonisothermal polymer processing operations. This problem was first considered by Marrucci[9] showing, for instance, that the term $D\ln T/Dt$ is coupled to the stress tensor, within the context of the kinetic theory of the dumbbell model. This idea was then discussed in the literature by Gupta and Metzner[20] and

Bird[10] and also extended to other rheological models such as the PTT (Sugeng et al.[15]). In the particular case in which the connector force between beads is proportional to temperature, a time derivative that considers the rate of thermal change can be defined as a first approximation through eq 13.[9,21]

Because both rheological models get the linear viscoelastic response at the asymptotic limit of small shear rates, the relaxation time λ_0 can be expressed as $\lambda_0 = 0.016 \exp[-11.9755 + 6802/(T + 273)]$ as reported by Gregory and Watson.[22] In particular, the PTTM considers a relaxation time that is a function of the stress tensor expressed as $\lambda = \lambda_0(T)/K(T,tr\boldsymbol{\tau})$ where $K = \exp[\xi tr\boldsymbol{\tau}/G]$. In this context of analysis, the relaxation modulus is also allowed to change with temperature according to $G = G_0(T/T_r)$ where T_r is the reference temperature.

Rheometric characterizations of these rheological models were carried out by following the same procedure described by Ottone and Deiber[8] to evaluate the rheological parameters of the PET melt (case study of this work) with experimental data reported by Gregory and Watson[22] involving the shear rate flow of a sample that had the same intrinsic viscosity as that of PET used by George[23] (zero shear rate viscosity $\eta_0 \approx 104.9$ Pa s). The results obtained are $\alpha \approx 0.85$ and $\alpha' \approx 4 \times 10^{-5}$ for the GM and $\alpha \approx 0.8$, $\chi \approx 4 \times 10^{-5}$, and $\xi \approx 9.25 \times 10^{-5}$ for the PTTM (see also, Hatzikiriakos et al.[24]). As expected, the PTTM predicted lower values of the elongational viscosity for an elongational rate greater than 30 s^{-1}.

Perturbation Analysis

We use the regular perturbation scheme proposed by Henson et al.[4] to obtain the perturbed 2D model. This scheme allows one to neglect rigorously terms of small orders from the balance and constitutive equations and the boundary conditions of the complete model. Then the perturbed 2D model is averaged in the radial direction of the filament, without any approximation, to yield an appropriate version of the perturbed average model.

The complete model described by eqs 1−13 can be expressed in dimensionless form by using the appropriate scales.[4] The perturbation analysis is carried out on the dimensionless model. Therefore, any dependent variable, represented by P in the generalized sense, can be expressed as $P = \sum_{n=0}^{\infty} \Lambda^n P^{(n)} = P^{(o)} + \vartheta(\Lambda)$. In the regular perturbation analysis, terms of order Λ and greater order are neglected to introduce the slenderness hypothesis. We will show below that further hypotheses are required to compute in a consistent manner the 1D conventional model and the hybrid 1D fluid mechanics/2D thermal model.

Before writing the resulting equations of the perturbed 2D model, we must introduce first a coordinate transformation to consider the axial variation of the filament radius $r_0(z)$. Thus, we define new coordinates $Z = z$ and $\zeta = r/r_0(z) = r/r_0(Z)$ to obtain a rectangular computational domain.[5,25] It should be observed that this transformation together with the kinematics of spinning and its boundary conditions are appropriate to compute fully the convective operator $[v_z\,(\partial/\partial z) + v_r\,(\partial/\partial r)]$ in the simpler form $v_z\,(\partial/\partial Z)$.

Perturbed 2D Model. The resulting perturbed 2D model is then written by dropping the super index (o) to avoid a complex nomenclature, although a first-order perturbation is still implied. Because the resulting kinematics of the spinning flow is $v_z = v_z(Z)$ and $v_r = -(1/2)r_0(Z)\,\zeta\,(\partial v_z/\partial Z)$, the following momentum balances are obtained:

$$\frac{1}{\zeta}\frac{\partial}{\partial \zeta}(\zeta \tau^{rr}) - \frac{\tau^{\theta\theta}}{\zeta} - \frac{\partial p}{\partial \zeta} = 0 \tag{14}$$

for the r component and

$$\rho v_z \frac{\partial v_z}{\partial Z} = \frac{1}{r_0(Z)\,\zeta}\frac{\partial}{\partial \zeta}(\zeta \tau^{rz}) + \frac{\partial \tau^{zz}}{\partial Z} - \frac{\partial p}{\partial Z} + \rho g \tag{15}$$

for the z component. In the same context of analysis, the energy balance is

$$\rho c_v\left(v_z \frac{\partial T}{\partial Z}\right) = \frac{1}{r_0^{\,2}(Z)\,\zeta}\frac{\partial}{\partial \zeta}\left(\zeta k_s \frac{\partial T}{\partial \zeta}\right) + (\tau^{zz} - \tau^{rr})\frac{\partial v_z}{\partial Z} \tag{16}$$

Also the PTTM can be expressed as

$$\tau_p^{zz}\frac{K}{\lambda_0} + v_z \frac{\partial \tau_p^{zz}}{\partial Z} - 2\frac{\partial v_z}{\partial Z}(1-\chi)\tau_p^{zz} - \tau_p^{zz}\left(\frac{v_z}{T}\frac{\partial T}{\partial Z}\right) - 2G\frac{\partial v_z}{\partial Z} = 0 \tag{17}$$

$$\tau_p^{rr}\frac{K}{\lambda_0} + v_z \frac{\partial \tau_p^{rr}}{\partial Z} + \tau_p^{rr}\frac{\partial v_z}{\partial Z}(1-\chi) - \tau_p^{rr}\left(\frac{v_z}{T}\frac{\partial T}{\partial Z}\right) + G\frac{\partial v_z}{\partial Z} = 0 \tag{18}$$

Through a similar analysis, the GM yields

$$\frac{\tau_p^{zz}}{\lambda_0} + v_z \frac{\partial \tau_p^{zz}}{\partial Z} - 2\frac{\partial v_z}{\partial Z}\tau_p^{zz} - \tau_p^{zz}\left(\frac{v_z}{T}\frac{\partial T}{\partial Z}\right) + \frac{\alpha'}{G\lambda_0}(\tau_p^{zz})^2 - 2G\frac{\partial v_z}{\partial Z} = 0 \tag{19}$$

$$\frac{\tau_p^{rr}}{\lambda_0} + v_z \frac{\partial \tau_p^{rr}}{\partial Z} + \tau_p^{rr}\frac{\partial v_z}{\partial Z} - \tau_p^{rr}\left(\frac{v_z}{T}\frac{\partial T}{\partial Z}\right) + \frac{\alpha'}{G\lambda_0}(\tau_p^{rr})^2 + G\frac{\partial v_z}{\partial Z} = 0 \tag{20}$$

In addition, for both models $\tau_p^{rr} = \tau_p^{\theta\theta}$.

The initial conditions at $Z = 0$ for the perturbed 2D model are obtained directly from eq 4, while boundary conditions at the center line of the filament still require the constraint of symmetry but now in relation to the new coordinate ζ. The boundary conditions at the free surface are, however, significantly simplified because of the first-order perturbation applied to the complete model. Thus, for $\zeta = 1$ and any value of $Z = 0$, one obtains

$$v_r - \frac{\partial r_0}{\partial Z} v_z = 0 \tag{21}$$

$$v_z = v_{az} \tag{22}$$

$$\tau^{zr} = (\tau^{zz} - \tau^{rr})\frac{\partial r_0}{\partial Z} - \tau_a^{nt} \tag{23}$$

$$p - \tau^{rr} = \frac{\sigma}{r_0} + p_a \tag{24}$$

$$\frac{k_s}{r_0}\frac{\partial T}{\partial \zeta} = -h_e(T - T_a) \tag{25}$$

where $r_0 \equiv r_0(z) \equiv r_0(Z)$ throughout this work. Equation 21 is considered in the coordinate transformation to express the convective terms of stresses and temperature through $v_z\,(\partial/\partial Z)$, and the use of eqs 23 and 24 is crucial to obtain a precise averaged balance of moments as reported below. Also, at position $Z = L$, where the fiber reaches the glassy temperature, one requires $v_z = v_L$ and $T = T_g$, where v_L is the tangential take-up velocity.

Perturbed Average Model. The numerical algorithm proposed in this work requires a rigorous averaging in the radial direction of eqs 14−20. The radial average is defined as follows:

$$\langle P\rangle = 2\int_0^1 P(Z,\xi)\,\xi\,d\xi \tag{26}$$

to obtain a set of equations that conforms to the perturbed average model. Thus, the continuity equation $(\nabla\cdot\mathbf{v}) = 0$ is better expressed, for practical reasons, as a macroscopic balance at any position Z according to $\rho\pi r_0^2 v_z = m$, where m is the mass flow rate in the extrusion capillary. From eqs 14, 15, 23, and 24, the averaged momentum balance is obtained as follows:

$$\rho v_z\frac{\partial v_z}{\partial Z} = \frac{2}{r_0}\left[(\langle\tau^{zz}\rangle - \langle\tau^{rr}\rangle)\frac{\partial r_o}{\partial Z} - \tau_a^{zr}\right] + \frac{\partial\langle\tau^{zz}\rangle}{\partial Z} - \frac{\partial\langle\tau^{rr}\rangle}{\partial Z} + \rho g + \frac{\sigma}{r_0^2}\frac{\partial r_0}{\partial Z} \tag{27}$$

In eq 27 we can express $\tau_a^{zr} = C_f\rho_a v_z^2/2$, where ρ_a is the air density and C_f is the friction coefficient, between filament and air, varying with the axial position Z. This coefficient is evaluated through the correlation $C_f = 2\beta\text{-}(\eta_a/2\rho_a v_z r_0)^{0.61}$, where η_a is the air viscosity.[26] In this work, we obtained $\beta = 0.335$ for the GM and $\beta = 0.32$ for the PTTM. These values are within the admissible range $0.3 \le \beta \le 0.6$ usually reported in the literature.[26,27] From eq 16, the averaged energy balance is

$$\rho v_z\left(a\frac{\partial\langle T\rangle}{\partial Z} + b\left\langle T\frac{\partial T}{\partial Z}\right\rangle\right) = -\frac{2h}{r_0}(\langle T\rangle - T_a) + (\langle\tau^{zz}\rangle - \langle\tau^{rr}\rangle)\frac{\partial v_z}{\partial Z} \tag{28}$$

where $\langle T\rangle$ is the average filament temperature at position Z. Therefore, the overall heat-transfer coefficient $h = (1/h_e + 1/h_i)^{-1}$, which varies with the axial position, shall be expressed as a combination of the internal h_i and external h_e heat-transfer coefficients. To evaluate the external coefficient, we use $2h_e r_0/k_a = \beta Pr^{1/3}Re^{0.39}[1 + 64(v_{ar}/v_z)^2]^{0.166}$ as proposed by Denn,[26] where v_{ar} is the air transversal velocity, k_a is the air thermal conductivity, and $Re = 2v_z r_0\rho_a/\eta_a$ is the air Reynolds number that varies axially. The Prandtl number Pr is approximately 0.684 for air at 30 °C. The internal heat-transfer coefficient h_i at each axial position can be obtained from the knowledge of the temperature field provided by the local balance of energy given by eq 16.

The resulting averaged rheological equations are

$$\left\langle\tau_p^{zz}\frac{K}{\lambda_0}\right\rangle + v_z\frac{\partial\langle\tau_p^{zz}\rangle}{\partial Z} - 2\frac{\partial v_z}{\partial Z}(1-\chi)\langle\tau_p^{zz}\rangle - v_z\left\langle\frac{\tau_p^{zz}}{T}\frac{\partial T}{\partial Z}\right\rangle - 2\langle G\rangle\frac{\partial v_z}{\partial Z} = 0 \tag{29}$$

$$\left\langle\tau_p^{rr}\frac{K}{\lambda_0}\right\rangle + v_z\frac{\partial\langle\tau_p^{rr}\rangle}{\partial Z} + \frac{\partial v_z}{\partial Z}(1-\chi)\langle\tau_p^{rr}\rangle - v_z\left\langle\frac{\tau_p^{rr}}{T}\frac{\partial T}{\partial Z}\right\rangle + \langle G\rangle\frac{\partial v_z}{\partial Z} = 0 \tag{30}$$

for the PTTM and

$$\left\langle\frac{\tau_p^{zz}}{\lambda_0}\right\rangle + v_z\frac{\partial\langle\tau_p^{zz}\rangle}{\partial Z} - 2\frac{\partial v_z}{\partial Z}\langle\tau_p^{zz}\rangle - v_z\left\langle\frac{\tau_p^{zz}}{T}\frac{\partial T}{\partial Z}\right\rangle + \alpha'\left\langle\frac{(\tau_p^{zz})^2}{G\lambda_0}\right\rangle - 2\langle G\rangle\frac{\partial v_z}{\partial Z} = 0 \tag{31}$$

$$\left\langle\frac{\tau_p^{rr}}{\lambda_0}\right\rangle + v_z\frac{\partial\langle\tau_p^{rr}\rangle}{\partial Z} + \frac{\partial v_z}{\partial Z}\langle\tau_p^{rr}\rangle - v_z\left\langle\frac{\tau_p^{rr}}{T}\frac{\partial T}{\partial Z}\right\rangle + \alpha'\left\langle\frac{(\tau_p^{rr})^2}{G\lambda_0}\right\rangle + \langle G\rangle\frac{\partial v_z}{\partial Z} = 0 \tag{32}$$

for the GM. In eqs 29−32, we have rather complex average quantities that must be calculated with the pointwise balance of energy and constitutive equations in the numerical method proposed below, without introducing additional hypotheses.

For the perturbed average model, one imposes the following conditions:

$$v_z = v_s,\quad \langle T\rangle = T_0$$

$$r_0(0) = r_s,\quad \langle\tau^{zz}\rangle = \tau_0,\ \mathrm{Rel} = \frac{\langle\tau^{rr}\rangle}{\langle\tau^{zz}\rangle} \tag{33}$$

at $Z = 0$ and

$$\langle T\rangle = T_g,\quad v_z = v_L \tag{34}$$

at $Z = L$.

At this step, we have two sets of equations relevant for the numerical algorithm described in the appendix. One involves eqs 16−20 and the remaining boundary condition (eq 25) to calculate the temperature and stress fields axially and radially, and the other composes a first-order system of differential equations (eqs 27−32) with the constraints given by eqs 33 and 34. These two sets are the basis of our numerical scheme described in the appendix.

Results and Discussion

It is clear that the rigorous solution of the perturbed average model with nonisothermal viscoelastic constitutive equations expressed as a system of differential equations, $\dot{\mathbf{x}} = \mathbf{A}^{-1}(\mathbf{x})\cdot\mathbf{b}$, is rather difficult to obtain because the averages of nonlinear terms are unknown. In this sense, it is interesting to point out that in order to be able to formulate and solve the 1D conventional model, and also the so-called hybrid models mentioned above, one has to carry out additional approximations to generate a consistent system of first-order differential

equations that may be solved through the Runge−Kutta method. These conditions consider that the values of the averaged stresses are close to the values evaluated at the filament−air interface. Thus, stresses must be calculated at the average temperature $\langle T\rangle$ with the consequence that their radial resolutions are lost (the skin−core structure cannot be predicted). In this context of analysis, when one is more interested in the evolution of macroscopic variables concerning the spinning operation, the following approximations associated with the determination of the stress tensor are useful (see eqs 28−32):

$$\langle \boldsymbol{\tau}(\partial \ln T/\partial Z)\rangle \approx \boldsymbol{\tau}(\langle T\rangle)\,\partial \ln \langle T\rangle/\partial Z,$$

$$\langle \boldsymbol{\tau}^2/G\lambda_0\rangle \approx \boldsymbol{\tau}^2(\langle T\rangle)/[G(\langle T\rangle)\lambda_0(\langle T\rangle)],$$

$$\langle \boldsymbol{\tau}K/\lambda_0\rangle \approx \boldsymbol{\tau}(\langle T\rangle)K(\langle T\rangle)/\lambda_0(\langle T\rangle), \quad \langle \boldsymbol{\tau}/\lambda_0\rangle \approx \boldsymbol{\tau}(\langle T\rangle)/\lambda_0(\langle T\rangle)$$

Under these approximations, the conventional 1D model can be solved and hybrid models can provide an estimation of the radial resolution of temperature alone. Although good predictions of practical variables such as axial velocity and average temperature can be obtained with these approximations, more precise calculations are required to explore details of the filament microstructure. For instance, by solving the numerical algorithm proposed here for the PET as a case study, Figure 2 shows that numerical predictions of v_z and $\langle T\rangle$ along the filament with either the PTTM or the GM compare well with experimental data reported by George.[23] It is interesting to point out here that Doufas and McHugh[28] also obtained a good prediction for the same case study in this work by considering a small FIC (degrees of crystalline phase are on the order of 10^{-4}). All of these results are consistent in the sense that PET does not crystallize appreciably in normal melt spinning; at least the spinning speed is about 4000 m/min or more.[29]

Figure 3a shows that the formation of a skin−core structure is predicted with the numerical algorithm of the viscoelastic spinning model studied here. In fact, one observes that for a take-up velocity of 3000 m/min the stress difference increases toward the filament free surface in around 34% for the PTTM and 36% for the GM as a consequence of a small radial decrease of the temperature field (Figure 3b). Figure 4 provides a 2D representation of the lines with a constant stress difference to illustrate better this phenomenon. It is also relevant to point out here that the temperature profile predicted with the PTTM presents a small difference from that provided by the numerical solution with GM, mainly for high values of Z. This result is due to the coupling effect between the air-friction coefficient and the heat-transfer coefficient through parameter β (see work by Denn[26]), which is greater for GM ($\beta = 0.335$) than for PTTM ($\beta = 0.32$). In addition, this coupling effect also indicates that, although the GM yields an elongational viscosity higher than that of the PTTM for elongational rates greater than 30 s^{-1}, clearly the mechanical power term is not enough to cancel out the coupling effect through parameter β. It was observed numerically that thermal and mechanical predictions are very sensitive to this parameter and, of course, different rheological models require different values of β to fit appropriately the available experimental data.

Although numerical predictions for the two rheological models used here are in good agreement with experimental data involving velocity and average temperature, these models predict, however, different stress fields radially and axially in the filament. The additional result is that different polymer chain conformations are obtained in the filament, with this aspect depending on the choice of rheological models and on the degree of rheometric information one has available for the evaluation of rheological parameters. In this sense, particular emphasis should be placed on the rheometric characterization of the polymer to be processed by combining shear, elongational, and dynamic experimental data in the determination of rheological parameters.

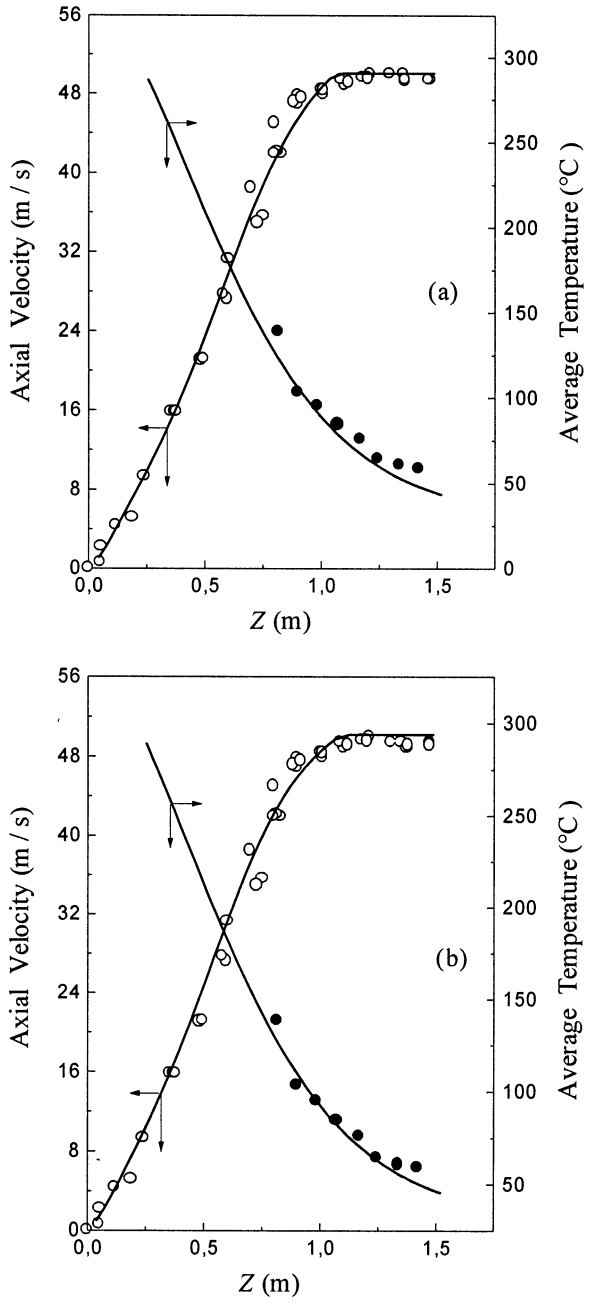

Figure 2. Numerical predictions of axial spinning velocity v_z and average temperature $\langle T\rangle$ for the PET case study: (a) GM; (b) PTTM. Open and full circles refer to experimental data of George[23] for a take-up velocity of 3000 m/min.

Figure 5 shows the evolution of the relative chain extension $\sqrt{tr\boldsymbol{\tau}/3G}$ and illustrates that chain extensions are rather poor near the center of the filament, while at the free surface high values of chain extension for the amorphous polymer are found. For the PET

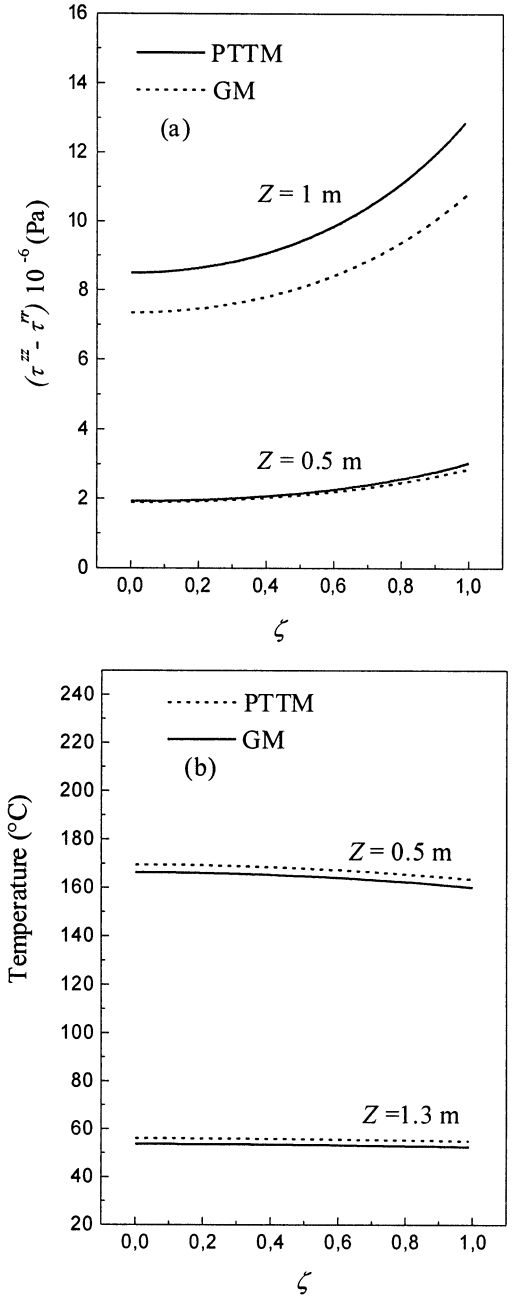

Figure 3. Numerical predictions with PTTM and GM of the radial variation of fields: (a) stress difference ($\tau^{zz} - \tau^{rr}$); (b) temperature T at two axial positions. The take-up velocity is the same as that in Figure 2.

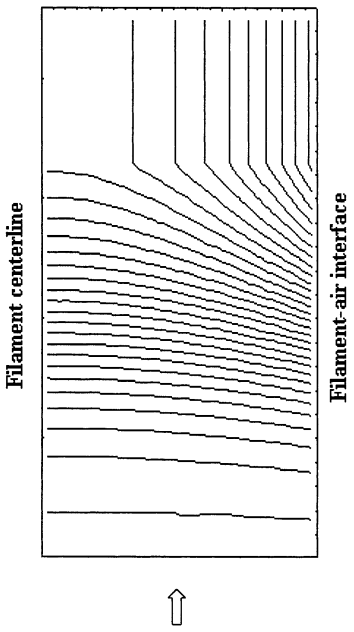

Figure 4. Lines of constant stress difference ($\tau^{zz} - \tau^{rr}$) predicted by the PTTM. The radial direction comprises $0 \le \zeta \le 1$, and the axial direction is within $0 \le Z \le L_T$. The plot contains 30 contour lines and has an aspect ratio of 2 to simulate the slenderness of the filament. The minimum value reported here is $(\tau^{zz} - \tau^{rr})_{min} = 10^4$ Pa, while the maximum value is $(\tau^{zz} - \tau^{rr})_{max} = 1.13 \times 10^7$ Pa. The take-up velocity is 3000 m/min.

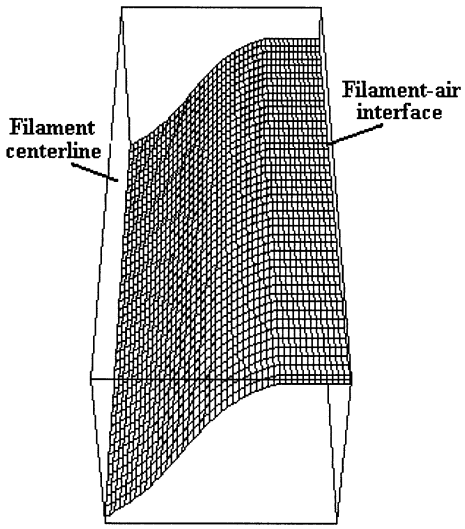

Figure 5. Tridimensional representation of the skin−core structure evaluated through the relative chain extension $\sqrt{tr\boldsymbol{\tau}/3G}$ with the PTTM. The maximum value is $(\sqrt{tr\boldsymbol{\tau}/3G})_{max} \approx 32$ at L_T. The take-up velocity is 3000 m/min.

studied here at a take-up velocity of 3000 m/min, we found that the PTTM yielded a maximum value $(\sqrt{tr\boldsymbol{\tau}/3G})_{max} \approx 32$ while with the GM this value was around 36. Although these values are relative in part to the rheological parameters used in the constitutive equations, mainly those involving the relaxation time and the shear modulus, it is clear that the microscopic stretching of polymer chains is rather small in relation to the macroscopic amount of stretch experienced by the filament at the draw ratio $DR = 165$. Therefore, extensive slippage of the entanglements within the polymer network is expected in agreement with previous results.[30]

Finally, although it is not reported here, we found that the skin−core structure and the relative chain extension increased significantly for lower values of the polymer thermal conductivity as a consequence of a sharper radial temperature profile obtained in the filament. Although our numerical method is formulated to introduce a thermal conductivity variable with the temperature (see eq 16), we have used an averaged value of k_s because the required information is not available in the literature at the present time.

Conclusions

More precise calculations than those reported with 1D models are required in fiber melt spinning to explore

details of the filament microstructure. For this purpose, the perturbed 2D model must be solved rigorously.

In the present work the main results are as follows: (1) A numerical method is proposed based on finite differences, allowing one to compute a high radial resolution of stresses and temperature at the precision desired (for instance, around 100 radial grid points). Also the classical approximations concerning the average of nonlinear terms are eliminated by using the analytical coupling between the perturbed average model resulting from the rigorous radial average of the perturbed 2D model and the associated pointwise energy balance and constitutive equations for stresses. (2) The constitutive equations used include the retarded elastic response allowing the computation of the flow domain from the maximum filament swelling. This effect was important to predict appropriately the filament velocity in the low speed range without crystallization. Thus, there was no need to include small crystallization effects in the PET to improve the prediction at low take-up velocity.[28] (3) Although different constitutive equations, like PTTM and GM, can fit well the same experimental data involving the average temperature and axial velocity of the filament, the stress fields obtained are different, yielding also different polymer chain conformations. This result indicates that the choice of constitutive equations should be carried out by placing more emphasis on the rheometric characterization of the material to be processed, mainly on those tests involving extensional flow. (4) The skin−core phenomenon was quantitatively predicted at low take-up velocities. (5) Although the heat transfer between cooling air and multifilament still requires further research because of the complex coupling between temperature and velocity fields of both phases, we found quantitatively that for the particular case of a monofilament the coupling between air friction and heat transfer is very sensitive to the values of parameter β as indicated by Denn[26] and, of course, different rheological models require different β to fit appropriately the experimental data available. (6) The numerical algorithm considers thermophysical properties and rheological parameters that depend pointwise on temperature.

Appendix: Numerical Solution by Finite Differences

To compute the perturbed 2D model coupled to the perturbed average model, here we present the main considerations to be accounted for in the construction of the numerical algorithm written in finite differences. First, the perturbed averaged model can be expressed in the matrix form $\dot{\mathbf{x}} = \mathbf{A}^{-1}(\mathbf{x})\cdot\mathbf{b}$ where

$$\dot{\mathbf{x}} = \left\{\frac{\partial v_z}{\partial Z}, \frac{\partial f}{\partial Z}, \frac{\partial \langle \tau_p^{zz}\rangle}{\partial Z}, \frac{\partial \langle \tau_p^{rr}\rangle}{\partial Z}, \frac{\partial \langle T\rangle}{\partial Z}\right\}$$

and $f = dv_z/dZ$.[8,31] It is then clear that these equations require the stress fields $\tau^{zz}(Z,\zeta)$ and $\tau^{rr}(Z,\zeta)$ and the temperature field $T(Z,\zeta)$ to evaluate the nonlinear averages indicated with $\langle\cdot\rangle$ and involved in matrix $\mathbf{A}^{-1}(\mathbf{x})$ (see eqs 28−32). Equation $\dot{\mathbf{x}} = \mathbf{A}^{-1}(\mathbf{x})\cdot\mathbf{b}$ can be written in finite differences by using the fourth-order Runge−Kutta method[32] to get the discrete vector $\mathbf{x}$. Therefore, from the perturbed 2D model, we calculate the temperature field from eq 16 written in finite differences.[33] The resulting tridiagonal matrix for the unknown values of temperatures at the grid points requires the discrete temperature value at the free surface, which can be calculated from eq 25 through a Taylor series expansion. In this algorithm N is the maximum number of nodes taken for the radial coordinate. In addition, the stress fields from the PTTM (eqs 17 and 18) can be written in the explicit−implicit finite differences for each axial position Z and any ζ. Similar equations can be derived for the stress fields obtained from the GM (eqs 19 and 20). Therefore, the structure of the numerical algorithm consists of solving the temperature and stress fields to calculate the nonlinear averages and internal heat-transfer coefficient required in the perturbed average model, which in turn must be solved by the fourth-order Runge−Kutta method. These calculations are carried out iteratively at each axial step until the convergence criteria are satisfied for the evaluation of the temperature and stress fields and for the numerical consistency between the perturbed 2D and average model. The iterative process also requires two convergence criteria associated with the determination of the length L, where the glass temperature is reached and the filament moves with the take-up velocity. The sequence of calculations and the coupling between the perturbed 2D and average models can be readily visualized through the steps of the flow diagram presented below, where the iterative loops and the criteria for convergence are indicated. We also found that $r_s = 1.44r_c$ is the appropriate value for the comparison with numerical results, as suggested previously by George.[23] It is assumed that the filament continues cooling for $Z > L$ until the total length L_T is reached at the take-up roller.

The flow diagram of the numerical algorithm is composed of the following relevant steps:

(A) Input of Numerical Data. (1) Spinning data: v_c, r_c, r_s, T_0, T_g, DR, β, v_{ar}, T_a, $v_L = DRv_s$. (2) Rheological parameters: ξ, α, λ_{00}, G_0, χ, α'. (3) Thermophysical properties of polymer and air: $\boldsymbol{c}_v = a + bT$, ρ, k_s, ρ_a, η_a, k_a, Pr. (4) Numerical parameters: τ_0^{zz}, Rel, ΔZ, $\Delta\tau_0^{zz}$, $\Delta\zeta$, N, E_v, E_T, E_1, E_2, E_3, E_4. (5) Control #1.

(B) Iterative Numerical Procedure. (1) Initial conditions: eqs 33 and 34. (2) Control #2: $Z = Z + \Delta Z$. (3) Control #3. (4) Evaluation of a system of first-order differential equations $\dot{\mathbf{x}} = \mathbf{A}^{-1}(\mathbf{x})\cdot\mathbf{b}$ with the Runge−Kutta method. (5) Control #4. (6) Pointwise calculation of τ^{zz}, τ^{rr}, and T by finite difference: eqs 17 and 18 for the PTTM and eqs 19 and 20 for the GM. (7) Test 1:

$$\frac{1}{N}\left|\sum_{j=1}^{N}(T_{i,j}^{k+1} - T_{i,j}^{k})/T_{i,j}^{k}\right| \le E_1 \approx 10^{-6} \quad \text{and}$$

$$\frac{1}{N}\left|\sum_{j=1}^{N}(\tau_{i,j}^{k+1} - \tau_{i,j}^{k})/\tau_{i,j}^{k}\right| \le E_2 \approx 10^{-6}$$

where k indicates an iteration number. (8) If false, go to control #4 (step B-5). (9) Test 2:

$$|(\langle T\rangle_{RK}{}^{i} - \langle T\rangle_{PW}{}^{i})/\langle T\rangle_{RK}{}^{i}| \le E_3 \approx 10^{-6} \quad \text{and}$$

$$|(\langle \tau\rangle_{RK}{}^{i} - \langle \tau\rangle_{PW}{}^{i})/\langle \tau\rangle_{RK}{}^{i}| \le E_4 \approx 10^{-6}$$

In these equations subindex RK indicates a variable calculated with the Runge−Kutta method and PW stands for the variable obtained from the average of the pointwise fields in the finite difference grid. (10) If false, go to control #3 (step B-3). (11) Evaluation of averages and the internal heat-transfer coefficient from temper-

ature and stress fields:

$$\langle T\rangle, \langle \tau\rangle, \left\langle \frac{\tau}{\lambda_0}\right\rangle, \left\langle \frac{\tau^2}{G\lambda}\right\rangle, \left\langle \frac{\tau}{T}\frac{\partial T}{\partial z}\right\rangle, \langle G\rangle, \left\langle T\frac{\mathrm{d}T}{\mathrm{d}z}\right\rangle, \left\langle \tau\frac{K}{\lambda_0}\right\rangle, \langle \eta_s\rangle, \left\langle \frac{\mathrm{d}\eta_s}{\mathrm{d}T}\right\rangle, h_i$$

(12) Test 3: $|\langle T\rangle^i - T_g|/|T_g| \le E_T \approx 10^{-6}$, where i yields the number of axial steps used to reach L. (13) If false, go to control #2 (step B-2). (14) Test 4: $|v_z^i - v_L|/|v_L| \le E_v \approx 10^{-6}$. Here E_v and E_T are the small errors involving the averaged temperature and axial velocity. (15) If false, $\tau_0^{zz} = \tau_0^{zz} + \Delta\tau_0^{zz}$ and go to control #1 (step A-5).

(C) Cooling of the Solid Fiber. (1) Control #5. (2) $Z = Z + \Delta Z$. (3) Pointwise calculation of T by finite difference with eq 16 and constant axial velocity. (4) Test 5: Is $Z = L_T$? If false, go to control #5 (step C-1).

(D) Write and Plot of Results.

Acknowledgment

The authors are thankful for financial aid received from the CONICET (Consejo Nacional de Investigaciones Científicas y Técnicas, Argentina) PIP 4811/97 and the Secretaría de Ciencia y Técnica de la UNL (Universidad Nacional del Litoral, Argentina) Programación CAI+D 96.

Literature Cited

(1) Denn, M. M. Continuous Drawing of Liquids to form Fibers. *Annu. Rev. Fluid Mech.* **1980**, *12*, 365.

(2) Denn, M. M. In *Computational Analysis of Polymer Processing*; Pearson, J. R. A., Richardson, S. M., Eds.; Applied Science Publishers: New York, 1983.

(3) Schowalter, W. R. *Mechanics of Non-Newtonian Fluid*; Pergamon Press: New York, 1978.

(4) Henson, G. M.; Cao, D.; Bechtel, S. E.; Forest, M. G. A Thin-Filament Melt Spinning Model with Radial Resolution of Temperature and Stress. *J. Rheol.* **1998**, *42*, 329.

(5) Doufas, A. K.; McHugh, A. J. Two-Dimensional Simulation of Melt Spinning with a Microstructural Model for Flow-Induced Crystallization. *J. Rheol.* **2001**, *45*, 855.

(6) Doufas, A. K.; McHugh, A. J. A Continuous Model for Flow-Induced Crystallization of Polymer Melts. *J. Rheol.* **1999**, *43*, 85.

(7) Denn, M. M. Issues in Viscoelastic Flow. *Annu. Rev. Fluid Mech.* **1990**, *22*, 13.

(8) Ottone, M. L.; Deiber, J. A. Modeling the Melt Spinning of Polyethylene Terephthalate. *J. Elast. Plast.* **2000**, *32*, 119.

(9) Marrucci, G. The Free Energy Constitutive Equation for Polymer Solutions from the Dumbell Model. *Trans. Soc. Rheol.* **1972**, *16*, 321.

(10) Bird, R. B. Use of Simple Molecular Models in the Study of the Mechanical Behavior of Solutions of Flexible Macromolecules. *J. Non-Newtonian Fluid Mech.* **1979**, *5*, 1.

(11) Keunings, R.; Crochet, M. J.; Denn, M. M. Profile Development in Continuous Drawing of Viscoelastic Liquids. *Ind. Eng. Chem. Fundam.* **1983**, *22*, 347.

(12) Gagon, D. K.; Denn, M. M. Computer Simulation of Steady Polymer Melt Spinning. *Polym. Eng. Sci.* **1981**, *21*, 844.

(13) Denn, M. M.; Petrie, C. J. S.; Avenas, P. Mechanics of Steady Spinning of a Viscoelastic Liquid. *AIChE J.* **1975**, *21*, 791.

(14) Larson, R. G. *Constitutive Equations for Polymer Melts and Solutions*; Butterworth Series in Chemical Engineering; Butterworth Publishers: London, 1988.

(15) Sugeng, F.; Phan-Thien, N.; Tanner, R. I. A Study of Non-Isothermal Non-Newtonian Extrudate Swell by a Mixed Boundary Element and Finite Element Method. *J. Rheol.* **1987**, *31*, 37.

(16) Gordon, R. J.; Schowalter, W. R. Anisotropic Fluid Theory: A Different Approached to the Dumbbell Theory of Dilute Polymer Solutions. *Trans. Soc. Rheol.* **1972**, *16*, 79.

(17) Joseph, D. D.; Renardy, M.; Saut, J. C. Hyperbolicity and Change of Type in the Flow of Viscoelastic Fluids. *Arch. Ration. Mech. Anal.* **1985**, *87*, 213.

(18) Crochet, M. J. A. Nonisothermal Theory of Viscoelastic Materials. *Theoretical Rheology*; John Wiley & Sons: New York, 1975.

(19) Pearson, J. R. A.; McIntire L. V. Nonisothermal Rheology of Polymers and Its Significance in Polymer Processing. *J. Non-Newtonian Fluid Mech.* **1979**, *6*, 81.

(20) Gupta, R. K.; Metzner, A. B. Modeling of Nonisothermal Polymer Processes. *J. Rheol.* **1982**, *26*, 181.

(21) Fisher, R. J.; Denn, M. M. Mechanics of Nonisothermal Polymer Melt Spinning. *AIChE J.* **1977**, *23*, 23.

(22) Gregory, D. R.; Watson, M. T. Steady-State Properties of Poly(Ethylene Terephthalate) Melts. *J. Polym. Sci.* **1970**, *30*, 399.

(23) George, H. H. Model of Steady-State Melt Spinning at Intermediate Take-Up Speeds. *Polym. Eng. Sci.* **1982**, *22*, 292.

(24) Hatzikiriakos, S.; Heffner, G.; Vlassopoulos, D.; Christodoulou, K. Rheological Characterization of Polyethylene Terephthalate Resin Using Multimode Phan-Thien−Tanner Constitutive Relation. *Rheol. Acta* **1997**, *36*, 568.

(25) Deiber, J. A.; Schowalter, W. R. Flow through Tubes with Sinusoidal Axial Variations in Diameter. *AIChE J.* **1979**, *25*, 638.

(26) Denn, M. M. Correlations for Transport Coefficients in Textile Fiber Spinning. *Ind. Eng. Chem. Res.* **1996**, *35*, 2842.

(27) Ziabicki, A.; Kawai, H. *High-Speed Fiber Spinning*; John Wiley & Sons: New York, 1985.

(28) Doufas, A. K.; McHugh, A. Simulation of Melt Spinning Including Flow-Induced Crystallization. Part III. Quantitative Comparisons with PET Spinline Data. *J. Rheol.* **2001**, *45*, 403.

(29) Katayama, K.; Tsuji, M. Fundamental of Spinning. In *Advanced Fiber Spinning Technology*; Nakajima, T., Ed.; Woodhead Publishing Limited: Cambridge, England, 1996.

(30) Doufas, A. K.; McHugh, A. J.; Miller, Ch. Simulation of Melt Spinning Including Flow-Induced Crystallization. Part I. Model Development and Predictions. *J. Non-Newtonian Fluid Mech.* **2000**, *92*, 27.

(31) Papanastasiou, T. C.; Dimitriadis, V. D.; Scriven, L. E.; Macosko, C. W.; Sani, R. L. On the Inlet Stress Condition and Admissibility Condition of Fiber Spinning. *Adv. Polym. Technol.* **1996**, *15*, 237.

(32) Carnahan, B.; Luther, H. A.; Wilkes, J. O. *Applied Numerical Methods*; John Wiley & Sons: New York, 1969.

(33) Peaceman, D. W. *Fundamentals of Numerical Reservoir Simulation*; New York, 1977.

Received for review December 11, 2001
Revised manuscript received April 25, 2002
Accepted April 26, 2002

IE011001I